Effects of solvation and core switching on the photoelectron angular distributions from $(CO_2)_n^-$ and $(CO_2)_n^- \cdot H_2O$

Richard Mabbs, Eric Surber, Luis Velarde, and Andrei Sanov[a)]
Department of Chemistry, University of Arizona, Tucson, Arizona 85721-0041

(Received 3 December 2003; accepted 19 December 2003)

Photoelectron images are recorded in the photodetachment of two series of cluster anions, $(CO_2)_n^-$, $n=4-9$ and $(CO_2)_n^- \cdot H_2O$, $n=2-7$, with linearly polarized 400 nm light. The energetics of the observed photodetachment bands compare well with previous studies, showing evidence for switching between two anionic core structures: The CO_2^- monomer and covalent $(CO_2)_2^-$ dimer anions. The systematic study of photoelectron angular distributions (PADs) sheds light on the electronic structure of the different core anions and indicates that solvation by several CO_2 molecules and/or one water molecule has only moderate effect on the excess-electron orbitals. The observed PAD character is reconciled with the symmetry properties of the parent molecular orbitals. The most intriguing result concerns the PADs showing remarkable similarities between the monomer and dimer anion cluster-core types. This observation is explained by treating the highest-occupied molecular orbital of the covalent dimer anion as a linear combination of two spatially separated monomeric orbitals. © *2004 American Institute of Physics.*
[DOI: 10.1063/1.1647535]

I. INTRODUCTION

Photoelectron spectroscopy[1] allows the study of not only the electronic structure of negative ions and neutral molecules, but also the intermolecular interactions. Experiments on cluster anions examine the molecular-level interactions implicated in the chemistry of condensed environments, effectively bridging the gap between the gas and condensed phases.[2–4] The imaging approach[5,6] to photoelectron spectroscopy, recently implemented for molecular and cluster anions,[7–9] adds an extra dimension to these studies. In addition to increased detection efficiency for low kinetic energy electrons, the three-dimensional velocity distribution of the photoelectrons can be determined with relative ease. Photoelectron images unravel signatures of the molecular orbitals (MOs) from which detachment takes place and so information is provided about both the energy and structure of the electron orbitals of the parent anion.

In the work presented here, we pursue a detailed study of the photodetachment of carbon–dioxide cluster anions with a special emphasis on the photoelectron angular distributions (PADs). The focus of this investigation is the effect of intermolecular interactions implicated in solvation and covalent bonding on the electronic structure and related properties of the cluster anions in question. This work complements our recent photoelectron imaging studies of $(CS_2)_n^-$, $n=1-4$, $(OCS)_n^-$, $n=2-4$, and $OCS^-(H_2O)_n$, $n=1$ to 2 cluster anions.[7–11] The previous experiments corroborated the past evidence[12,13] for the existence of different types of core anion species within the $(CS_2)_n^-$ and $(OCS)_n^-$ clusters. In clusters of the first type, the excess electron resides on a single CS_2 or OCS moiety and thus the corresponding cluster structures are described as $CS_2^-(CS_2)_{n-1}$ and $OCS^-(OCS)_{n-1}$, respectively. In clusters of the second type, the electron occupies a molecular orbital (MO) of a covalently bound dimer anion and the corresponding cluster structures are described as $(CS_2)_2^-(CS_2)_{n-2}$ and $(OCS)_2^-(OCS)_{n-2}$, respectively.

Electron detachment from different core isomers in $(CS_2)_n^-$ was shown to give rise to distinct PADs.[8] In particular, 400 nm photodetachment from the monomer and dimer core isomers yielded PADs characterized by the anisotropy parameters (β) of opposite signs. This case is an unequivocal example of the combined angular and energy domain observations yielding clearly distinguishable signatures of different cluster types. In addition to the direct detachment transitions, the $(CS_2)_n^-$ and $(OCS)_n^-$ cluster anions also exhibit autodetachment (AD), which was attributed to the corresponding dimer-based isomers.[8,10,11,14] In agreement with this assignment, no AD was observed from the monomer anions of OCS clustered with one or two water molecules.[7]

The $(CS_2)_n^-$ and $(OCS)_n^-$ clusters belong to the same isovalent family as $(CO_2)_n^-$. Photoelectron spectroscopy of $(CO_2)_n^-$ and $(CO_2)_n^- \cdot H_2O$ revealed evidence for different anionic core structures within these clusters as well.[15–19] Johnson and co-workers noticed a discontinuity in the trend of vertical detachment energy (VDE) as a function of the $(CO_2)_n^-$ cluster size: A steady increase in VDE is observed from $n=2$ to 5, but VDE for $n=7$ is 0.65 eV lower than that for $n=5$—a pronounced effect ascribed to cluster core switching.[15] For $(CO_2)_6^-$, there is evidence of coexistence of two electronic isomers which possibly undergo interconversion.[17,20,21] Theoretical work[20,22,23] supports the contention that $(CO_2)_n^-$, $n=2-5$ clusters comprise of a covalently bound dimer anion core solvated by the remaining

a)Electronic mail: sanov@u.arizona.edu

neutral molecules: $(CO_2)_2^-(CO_2)_{n-2}$. For $n>6$, the cluster core switches to a monomer anion solvated by $(n-1)$ neutral CO_2 molecules. A similar picture emerges in $(CO_2)_n^- \cdot H_2O$, where the coexistence of different core types is seen for $n=2-4$, followed by an apparent switch to just one type (the monomer anion) for $n>4$.[16,18] Calculations indicate that there are several close lying structures associated with these isomers, but they all are either dimer or monomer based.[22,23]

In 1988, Johnson's group carried out several qualitative determinations of the angular anisotropy of the electrons ejected from $(CO_2)_n^-$ clusters and noted that the PADs were always strongly skewed along the laser polarization vector.[15] Recently, we performed a systematic imaging study of this cluster system. Our preliminary report[14] documented and quantified the striking similarity of the PADs originating from the solvated monomer and dimer anions of CO_2 and offered an explanation of this effect. The analysis was based on the linear-combination-of-molecular-orbitals (LCMO) description of the dimer anion's highest-occupied molecular orbital (HOMO), combined with the dual-source interference picture of the detachment process.[14] The objective of the current study is to characterize the effects of solvation, (mono) hydration, and core switching on the PADs from the cluster anions of carbon dioxide. This task has twofold importance. First, it provides experimental evidence of the localization of the excess electron to a small region of a larger cluster. Second, knowledge of the PADs from the monohydrated clusters is an important step in understanding how the structure of the excess electron changes upon increasing hydration.[24]

The paper is organized as follows. A brief description of the salient points of the experimental arrangement in the next section is followed by presentation of the images resulting from 400 nm photodetachment from a range of cluster anions in the $(CO_2)_n^-$ and $(CO_2)_n^- \cdot H_2O$ series. The electron kinetic energy (eKE) distributions are shown to be in good agreement with previous work. The PADs are characterized and interpreted in terms of the core anion structures and electron orbitals making use of quantum chemical calculation and the previously proposed *s&p* model of negative-ion photodetachment.[7,9] Finally, a brief discussion is made of the remarkable similarity in the PADs for CO_2 cluster anions with different cluster cores.

II. EXPERIMENT

The experimental apparatus is described in detail elsewhere.[9] In brief, it employs the ion generation and mass analysis techniques of Lineberger and co-workers,[25,26] which are combined with a velocity mapped,[27] imaging[5] scheme for detection of the photoelectrons.

The $(CO_2)_n^-$ and $(CO_2)_n^- \cdot H_2O$ clusters are formed by expansion of undried CO_2 at a stagnation pressure of 0–20 psig through a pulsed (70 Hz) nozzle (General Valve Series 9) into a region with a base pressure of 10^{-6} Torr (rising to 2×10^{-5} Torr when the valve is operated). The supersonic expansion is crossed with a 1 keV electron beam and the anions are pulse extracted into a Wiley–McLaren time-of-flight mass spectrometer.[28] The ions enter the detection region with a typical base pressure of $3-5\times10^{-9}$ Torr. Mass selection is ensured by ion detection using a dual microchannel plate (MCP) detector (Burle, Inc.) situated at the very end of the apparatus.

The ion beam is crossed with the frequency doubled output beam from an amplified Ti:Sapphire laser system (Spectra Physics, Inc.) producing 1 mJ, 100 fs pulses at 800 nm. Frequency doubling a portion of the fundamental output using a BBO crystal produces 400 nm radiation at 120 μJ/pulse. The linearly polarized laser beam is mildly focussed using a 2 m focal length lens positioned ~1.3 m before the laser beam crosses the ion beam.

Photoelectron detection takes place in the direction perpendicular to the ion and laser beams. A 40 mm diameter MCP detector with a P47 phosphor screen (Burle, Inc.) is mounted at the end of an internally μ-metal shielded electron flight tube. Images are obtained from the phosphor screen using a CCD camera (Roper Scientific, Inc.) and are typically averaged for $1-3\times10^4$ experimental cycles. To discriminate against experimental background, the potential difference across the two imaging MCPs, normally maintained at 1.0–1.2 kV, is pulsed up to 1.8 kV for a 200 ns window timed to coincide with the arrival of the photoelectrons.

III. RESULTS AND ANALYSIS

The 400 nm photoelectron images of $(CO_2)_n^-$ and $(CO_2)_n^- \cdot H_2O$ are shown in Fig. 1. They correspond to two-dimensional projections of the three-dimensional distributions of the emitted electrons onto the plane of the detector. The electron detachment process is cylindrically symmetric with respect to the laser polarization direction, defined as the laboratory-frame *z* axis (vertical axis in the plane of all images). The kinetic energy and angular distributions of the photoelectrons are reconstructed using the BAsis-Set EXpansion (BASEX) inverse-Abel transform method developed by the Reisler group.[29]

Upon inspection of Fig. 1, strong similarities are apparent between the images in the two series. In particular, all PADs peak in the vertical direction, along the laser polarization axis. The spot seen at the center of the $(CO_2)_2^- \cdot H_2O$ image is unusual in that it is laser-independent and can possibly be attributed to field-detachment of metastable cluster anions. We have also observed this phenomenon in $CO_2^-(H_2O)_{1,2}$.[24] In the current work, analysis of the $(CO_2)_2^- \cdot H_2O$ image is carried out after subtraction of the laser-independent signal (marked *ii* in Fig. 1), yielding the photo-induced image (marked *i* in Fig. 1).

A. Photoelectron spectra

To a certain extent, the relative abundance of a particular cluster core-type (especially in the case of mixed clusters) depends upon the ion source conditions. Since discussion of the PADs (Sec. IV) will be based upon the structural conclusions drawn in earlier studies, it is important to verify that the major structural trends involved in our measurements are the same. At a qualitative level, the evidence for core switching is easy to see from the size of the images. The imaging conditions (most pertinently the electron lens voltages)[9,27]

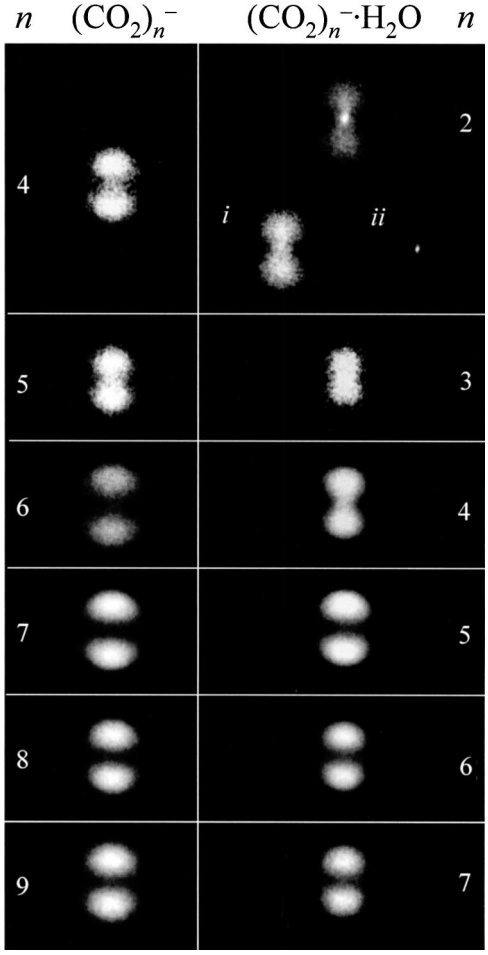

FIG. 1. Electron detachment images of carbon–dioxide cluster anions. The left-hand column represents the nonhydrated series, while the right-hand column represents the monohydrated series. The laser wavelength is 400 nm and the laser polarization direction is vertical in the figure plane. The $(CO_2)_2^-\cdot H_2O$ image shows a laser-independent feature at the center. The photo-induced image (*i*) is shown below the experimental image after subtraction of the laser-independent signal (*ii*). All images were acquired using the same electron imaging lens voltages and are shown to scale.

are the same for all images shown in Fig. 1. Despite this, in the $(CO_2)_n^-$ series the image for $n=6$ covers a larger portion of the detector than that for $n=5$. The presence of faster electrons suggests a lower detachment threshold for the larger-size cluster. The same behavior is seen in the $(CO_2)_n^-\cdot H_2O$ series between $n=3$ and 4.

Photoelectron energy spectra extracted from the images were fitted by a sum of contributions accounting for detachment transitions from two different species:[15,17,18]

$$P(\mathrm{eKE}) = \mathrm{eKE}^{1/2}\{A_\mathrm{I}\exp[-(\mathrm{eBE}-\mathrm{VDE_I})^2/w_\mathrm{I}^2] + A_\mathrm{II}\exp[-(\mathrm{eBE}-\mathrm{VDE_{II}})^2/w_\mathrm{II}^2]\}, \quad (1)$$

where $\mathrm{eBE}=h\nu-\mathrm{eKE}$ is the electron binding energy, w_I and w_II are the half-width parameters of the Gaussians used to describe the Franck–Condon profiles of the individual bands. These parameters are related to the full widths at half-maxima (FWHM) as $\mathrm{FWHM}=2(\ln 2)^{1/2}w$. The pre-exponential factors A_I and A_II are proportional to the populations of the respective core ions, as well as the cross sections for the corresponding transitions. The imaging technique allows efficient detection of low energy electrons, for which threshold effects are important. These effects are accounted for by the approximate scaling factor $\mathrm{eKE}^{1/2}$ included in Eq. (1), which reflects a Wigner-type near-threshold behavior for partial waves with the orbital angular momentum quantum number $\ell=0$. More restrictive near-threshold scaling of higher-order waves is neglected in the model described by Eq. (1).

TABLE I. The VDE and FWHM values (in eV) for bands I and II, corresponding to cluster anions with monomer (I) and dimer (II) cores, respectively, used to fit the photoelectron energy spectra: (a) this work (spectra obtained from the images in Fig. 1); (b) from Ref. 15; (c) from Ref. 18.

		$(CO_2)_n^-$				$(CO_2)_n^-\cdot H_2O$			
	Core	VDE		FWHM		VDE		FWHM	
n	type	(a)	(b)	(a)	(b)	(a)	(c)	(a)	(c)
2	II					3.41	3.39	1.21	1.30
	I					2.20	2.14	0.92	0.97
3	II					3.54	3.49	1.13	1.30
	I					2.38	2.38	0.93	0.97
4	II	2.96	2.96	1.00	0.96	3.71	3.71	1.16	1.30
	I					2.63	2.63	1.03	0.97
5	II	3.25	3.25	1.07	1.06				
	I					2.77	2.77	1.07	1.11
6	II	3.40	3.40	0.73	0.73				
	I	2.49	2.49	0.98	0.98	2.94	2.92	1.02	0.99
7	I	2.62	2.62	0.97	0.92	3.04		0.92	
8	I	2.80	2.73	0.92	0.92				
9	I	2.92	2.80	0.92	0.87				

The VDE and FWHM fitting parameters for bands I and II are summarized in Table I, where they are compared with the values reported in earlier studies. A good agreement is observed, the only difference between the analysis in this study and previous work being the use of the $\mathrm{eKE}^{1/2}$ scaling factor in Eq. (1).

B. Angular distributions

The PADs resulting from the one-photon detachment using linearly polarized radiation can be described by the anisotropy parameter β,[30–32] which is, in general, energy dependent. This dependence may complicate comparison between different species, but meaningful insights can be gained by examining the variations in β across a chosen energy range. Figure 2 shows plots of energy-dependent β for representative monomer and dimer based, nonhydrated and hydrated cluster anions studied. In all cases, β is significantly positive and contained within a rather narrow range.

IV. DISCUSSION

The images in Fig. 1 yield energy-domain fitting parameters that are very close to those reported in earlier work.[15,18] Thus it is reasonable to base discussion of the observed PADs upon previously described cluster anion core structures.

There are two important comparisons to be made in the series of photoelectron images presented. The first is between the PADs corresponding to monomer versus dimer

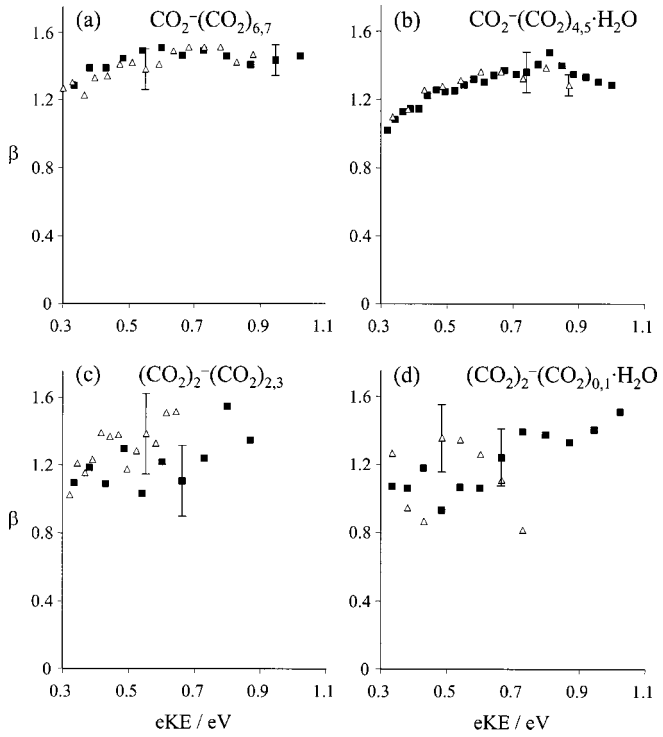

FIG. 2. The anisotropy parameter β as a function of eKE. (a) $(CO_2)_n^-$, the nonhydrated monomer-based cluster anions: ■ $n=7$, △ $n=8$. (b) $(CO_2)_n^-\cdot H_2O$ monohydrated monomer-based cluster anions: ■ $n=5$, △ $n=6$. (c) $(CO_2)_n^-$, nonhydrated dimer-based cluster anions: ■ $n=4$, △ $n=5$. (d) $(CO_2)_n^-\cdot H_2O$ monohydrated dimer-based cluster anions: ■ $n=2$, △ $n=3$. The error bars shown represent one standard deviation for a given dataset.

based clusters. This comparison sheds light on the electronic structures of the different cluster cores. The second is between the hydrated and nonhydrated cluster anions, highlighting the possible differences between the effects of hydration and solvation by carbon dioxide.

Figure 2 shows that for a given cluster-core type the β values at a given eKE are very similar, regardless of cluster size. This is particularly clear for the monomer-based clusters where (for example) the values for $n=7$ and 8 (nonhydrated), as well as for $n=5$ and 6 (hydrated) lie close to one another. For dimer-based clusters, the values for $n=4$ and 5 (nonhydrated), as well as for $n=2$ and 3 (hydrated) are also within one standard deviation for a given eKE.

A. Monomer vs dimer based clusters

Comparison between monomer and dimer based $(CO_2)_n^-$ clusters can be made by examining Figs. 2(a) and 2(c), respectively. The anisotropy values are generally slightly lower for the dimer-based clusters, but the difference is well within the standard deviations of the two datasets.

The corresponding comparison is less straightforward in the hydrated series, where the lower-n members are comprised of mixtures of the dimer and monomer based isomers.[18] Still, Fig. 2(b) represents the monomer-based clusters $CO_2^-(CO_2)_4\cdot H_2O$ and $CO_2^-(CO_2)_5\cdot H_2O$. Concerning the data in Fig. 2(d), the relative intensities of the monomer to dimer cores for $n=2$ and 3 were reported by Tsukuda *et al.* as 0.11 and 0.08 respectively.[18] In the current study, coefficients A_I and A_{II} in Eq. (1) are to a good approximation proportional to the abundances of the monomer and dimer cores, respectively. The A_I/A_{II} ratio is found to equal 0.19 for $n=2$ and 0.02 for $n=3$. Thus, in both the present work and that of Tsukuda *et al.* the major core species in the $(CO_2)_n^-\cdot H_2O$, $n=2$, 3 clusters is the dimer and hence the data in Fig. 2(d) correspond mainly to the dimer-anion core. Again, the dimer-based structures in the main show slightly lower β values, but both the monomer and dimer-based data overlap within one standard deviation over the entire energy range.

The similarity of the PADs emanating from the dimer and monomer based clusters in both the $(CO_2)_n^-$ and $(CO_2)_n^-\cdot H_2O$ series is perhaps the most intriguing result of this study. In direct photodetachment, the PAD relates to the structure of the parent MO, which is of particular interest for systems involving two or more electronic isomers. Given the different types of the ionic cores and HOMOs involved in the monomer and dimer based clusters, one intuitively expects these fundamental structural differences to be reflected in the PADs. Yet, despite the core switching, the images resulting from all clusters in both the $(CO_2)_n^-$, $n=4-9$ and $(CO_2)_n^-\cdot H_2O$, $n=2-7$ series indicate similar PADs (see Fig. 1). This observation is particularly significant in view of the recent results for isovalent $(CS_2)_n^-$, where the dimer and monomer based clusters give rise to markedly different bands in photoelectron images.[14] This discrepancy must be understood in terms of fundamental differences in the geometric and/or electronic structures of the dimer anions of CO_2 and CS_2.

The following discussion of the PADs originating from the monomer and dimer anion cores of $(CO_2)_n^-$ and $(CO_2)_n^-\cdot H_2O$ consists of two parts. First, we discuss the qualitative nature of the observed angular distributions, making use of the symmetry of the orbitals initially containing the detached electrons. Second, we analyze the PADs from the monomer and dimer anion cores within the framework of an LCMO description of the dimer anion HOMO and a dual-source interference picture of the photodetached electron waves.

1. Parallel nature of the CO_2^- and $(CO_2)_2^-$ PADs

The $\beta>0$ PAD character can be understood using the $s\&p$ model, which considers symmetry of the free electron waves allowed in the electric–dipole approximation. A detailed description of the model is given elsewhere,[9] accompanied by step-by-step applications to several molecular and cluster anions.[7,9,14] In brief, the photo-detached electron wave symmetry is determined under the molecular-orbital and electric–dipole approximations. The symmetry constraint combined with a chosen orientation of the anion dictates the partial wave composition of the free-electron wave function in the laboratory frame (LF). A further approximation neglects the components with the angular momentum quantum number $\ell>1$, limiting the discussion to s and p partial waves only (hence the name of the model).[9] The s and p waves determined by this procedure repeated for a small number of principal orientations of the anion are used to determine the PAD character.

In the cluster anions considered here the excess electron is localized on the monomer or dimer core. Consequently, it is the core anion symmetry that is relevant to the PADs obtained. Our initial discussion will assume that although the symmetry of the monomer or dimer anion core can be altered by solvation/hydration, their overall structures remain largely unchanged. Later, we will explore the validity of this assumption.

For the monomer-based clusters, the relevant core anion symmetry is C_{2v}. The $s\&p$ description of CO_2^- photodetachment follows closely the CS_2^- case, discussed in detail elsewhere.[9] As with CS_2^-, the HOMO containing the unpaired electron in CO_2^- belongs to the A_1 symmetry species. Considering electric–dipole transitions from the HOMO, three final-state symmetries are allowed for the photodetached electron: A_1, B_1, and B_2. These symmetry species are defined in the molecular frame (MF). The relative amplitudes depend on the orientation of the anion with respect to the laser field vector, defined in the LF. As shown previously,[9] under the $\ell \leqslant 1$ approximation the A_1, B_1, and B_2 symmetry waves correspond to *p* waves polarized preferentially in the *z* direction coinciding with the laser polarization, in addition to an *s* wave allowed only under the A_1 wave symmetry. These components overlap to give the final PAD pattern peaking along *z*.

A similar approach can be applied to the covalent dimer anion. Fleischman and Jordan predicted that this anion has a D_{2d} symmetry structure with two bent CO_2 units linked by a covalent (order of 1/2) C–C bond.[22] This structure and the corresponding HOMO are shown in Fig. 3(a.1). While the initial prediction was based on a HF/6-31+G calculation, the covalent dimer anion structure was later re-optimized by Saeki *et al.* at a higher MP2/6-31+G* and MP2/aug-cc-pVDZ levels and no deviation from D_{2d} symmetry was observed.[23]

Since the D_{2d} dimer HOMO corresponds to the A_1 irreducible representation, the allowed free-electron wave symmetries are B_2 and E, depending on the orientation of the anion relative to the laser polarization axis. The B_2 waves emanate from anion orientations with nonzero projections of the C–C bond axis on the LF *z* axis. In the *s* and *p* limit, the B_2 waves expand as *p* waves polarized along the C–C bond axis and predominantly along the *z* axis in the LF. The E symmetry waves are emitted from anions with nonzero perpendicular components of the C–C bond axis with respect to *z*. Again, *s* waves are not allowed, while the relevant *p* waves are polarized perpendicular to the C–C bond. In the LF these *p* waves may be polarized both in the *z* direction and perpendicular to it, making the predictions of the model less clear compared the monomer anion (C_{2v} symmetry) case. To arrive at more definitive conclusions supporting the parallel nature of the photodetachment process in the D_{2d} dimer anion one must evaluate the transition dipole matrix elements corresponding to different *p* waves.

The need for these calculations can be bypassed by considering the dimer anion structure within monohydrated clusters. As discussed below, the $(CO_2)_2^-$ core within these clusters is distorted from its D_{2d} symmetry. For example, in the structure shown in Fig. 3(b.1) the torsional angle between the two CO_2 groups is reduced to 75° due to the ionic hydrogen-bonding interaction of the water molecule with the dimer anion,[23] reducing its symmetry to C_2. Similarly, the dimer structure in Fig. 3(b.2) experiences a hydration-induced closing of the OCO angle, leading to symmetry change from D_{2d} to C_{2v}. In each case the dimer anion HOMO still conforms to the totally symmetric representation of the respective point group. Of the D_{2d}, C_2, and C_{2v} cases, the $s\&p$ description of the detachment process is least ambiguous for the C_{2v} group, where the free electron can be shown to include mixtures of *s* and *p* waves, the latter polarized predominantly along *z*.[9] Now consider that in all dimer anion structures discussed (the unperturbed D_{2d}, as well as the hydrated C_2 and C_{2v} structures) the detachment occurs from essentially the same HOMO. While the orbital is subject to solvent perturbations, their effect on its overall shape is not too great and the resulting PADs should be similar. Since the $s\&p$ analysis in the C_{2v} case unambiguously indicates a PAD peaking along the *z* axis, similar outcomes are expected in detachment from the $(CO_2)_2^-$ HOMO, regardless of the detailed cluster structure. Thus, positive photoelectron anisotropy is to be expected for all dimer-based $(CO_2)_n^-$ and $(CO_2)_n^- \cdot H_2O$ clusters studied.

2. Direct comparison of the CO_2^- and $(CO_2)_2^-$ PADs using the LCMO approximation

The application of the $s\&p$ model outlined above helps understand the parallel nature of the detachment process from both the monomer and dimer-based $(CO_2)_n^-$ and $(CO_2)_n^- \cdot H_2O$ cluster anions. However, this analysis does not explain the striking *quantitative* similarity between the β values in the photodetachment from the CO_2^- and covalent $(CO_2)_2^-$ cluster cores. The model gives merely an indication of the direction in which the PAD is expected to peak in each case, without embarking on direct comparison of the two qualitatively different core anion species. We now adopt a new approach, which allows for such comparison. The following discussion employs the conceptual framework outlined briefly in the previous discussion[14] of the differing electronic and structural properties of covalent $(CS_2)_2^-$ and $(CO_2)_2^-$.

We turn again to the $(CO_2)_2^-$ HOMO shown in Fig. 3(a.1). The orbital can be viewed as a combination of two spatially separated monomer–anion HOMOs, as sketched in Fig. 3(a.2). The LCMO (linear combination of molecular orbitals) formalism[33,34] allows the electron detachment to be thought of as a process emanating from two separated centers, each emitting waves characteristic of individual monomer units. As seen in Figs. 3(b.1) and 3(b.2), the core anion HOMO in larger dimer-based clusters can be approximated in the same manner.

Interference of waves emitted from two centers depends on the differential distance from each center along a given direction in the far-field limit, as well as the initial phase angle between the partial waves. The latter is subject to the constraints on the overall symmetry of the photodetached electron wave function. A discussion of the symmetry restrictions in the dual-center framework is given in our previous

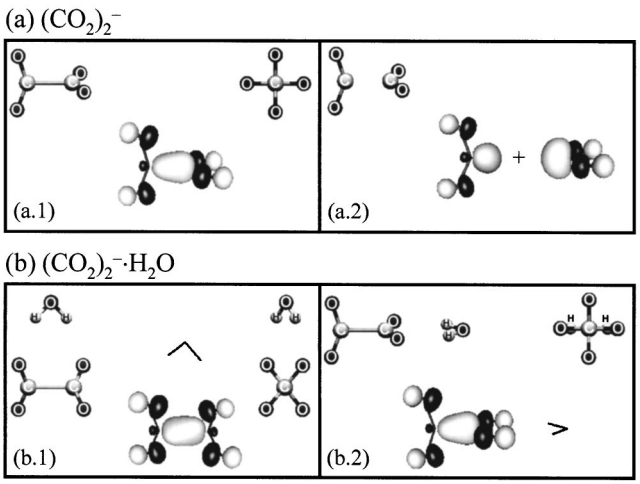

FIG. 3. Molecular-orbital plots representing the dimer-based cluster-anion HOMOs. (a.1) Isolated $(CO_2)_2^-$ D_{2d} symmetry covalent dimer anion. (a.2) LCMO representation of the dimer–anion HOMO shown in (a.1) as a superposition of two spatially separated monomeric orbitals. (b.1) Lowest-energy $(CO_2)_2^-\cdot H_2O$ structure, in which the core dimer–anion is distorted from D_{2d} to C_2 symmetry by the bridging H_2O group. (b.2) The $(CO_2)_2^-\cdot H_2O$ structure with H_2O in the end position. Geometries (shown next to the HOMO for each species) are taken from Ref. 23 and correspond to the potential minima calculated at the MP2 level of theory with the 6-31+G* basis set. The structures in (a.1), (b.1), and (b.2) are shown as viewed from two different directions: Perpendicular and along to C–C bond axis (top left and right corners of each frame, respectively).

report.[14] For the current discussion it suffices to note that the separation between the two monomer groups ($\leqslant 2$ Å) is small compared to the de Broglie wavelength of the emitted electrons calculated in the far field. This wavelength can be estimated, for example, as 14.6 Å at eKE=0.7 eV (corresponding to the middle of the relevant eKE range). Thus, the PAD arises from interference of waves emitted from two almost overlapping (on the electron-wavelength scale) centers. Under these conditions, the experimental observations are dominated by waves emitted with similar initial phases (constructive interference), while the waves interfering destructively are suppressed. In this framework, the PADs for CO_2^- and $(CO_2)_2^-$ can be compared directly and are expected to be similar as the free-electron wave function is roughly a sum of the in-phase components emitted from two monomer units.

B. Effects of solvation and monohydration

Comparing the data in the left and right columns of Fig. 2 sheds light on the effect of adding one water molecule to the monomer and dimer based cluster anions. The β values for hydrated and nonhydrated clusters are similar for a given eKE. Although the hydrated species tend to give slightly lower values than the nonhydrated species, the differences are within one standard deviation. The similarity indicates that the addition of one water molecule causes little perturbation of the shape of the HOMO of the ionic cluster core. This observation contrasts the preliminary findings of our ongoing studies, where increasing the number of H_2O molecules hydrating the CO_2^- anion has a pronounced effect on the PAD, causing the anisotropy to diminish.[24]

The insensitivity of the PADs to monohydration is similar to its insensitivity to stepwise solvation by CO_2. Both are supported by calculations of the HOMO structure under differing solvation conditions.

In previous work, Saeki *et al.* extended their theoretical [second-order Moller–Plesset (MP2)] study to $(CO_2)_n^-$, $n=3-6$ clusters by employing a smaller 6-31G basis set (compared to the 6-31+G* basis used by the authors for the dimer anion).[20] In these calculations, the dimer core geometry changed to a planar, (approximately) D_{2h} structure solvated by the remaining $n-2$ molecules. Intrigued by the change of core–anion symmetry from D_{2d} to D_{2h}, Saeki *et al.* re-optimized the geometry for $n=3$ using the 6-31+G* basis set and found that the inclusion of diffuse functions ''restored'' the predicted dimer–anion structure to the D_{2d} symmetry (slightly distorted by solvation) characteristic of the unsolvated dimer anion. Monohydrated cluster geometries were also determined at the MP2/6-31+G* level for $(CO_2)_n^-\cdot H_2O$, $n=1,2$.[23] For $n=1$, three potential minima were found; the corresponding structures are shown in Fig. 4(b). All are planar, with the C_{2v} structure [Fig. 4(b.1)] being the most stable. Six different structures were found for monohydrated $(CO_2)_2^-$, of which two correspond to covalent dimer anion clustered with H_2O [Fig. 3(b)] and the remainder are monomer anion based [Fig. 4(c)]. Again, the dimer-based structures are found to be the most stable and the one where the water molecule bridges the two ends of the dimer anion [Fig. 3(b.1)] has the lowest energy of the two.

Since the size of the basis set appears to be critical in determining the core anion symmetry, we investigated the structures and the HOMOs for $(CO_2)_n^-$, $n=2-4$ after geometry re-optimization at the MP2/6-311+G* level, using the structures determined by Saeki *et al.*[20,23] as starting points for our calculations.[35] We find that the dimer core anion in the most stable $(CO_2)_3^-$ cluster retains an approximate D_{2d} geometry when the larger basis set is used. Yet $(CO_2)_4^-$ has an approximately D_{2h} lowest-energy core structure, in agreement with the trend towards nearly D_{2h} core geometries indicated by Saeki's results.[20] However, the conclusions derived in the previous part of this section using the LCMO dual-source interference approach are unaffected by the ambiguity between the D_{2h} and D_{2d} geometries of the core anion, because the dimer–anion HOMO can be represented as a combination of the same two monomer–anion orbitals in either case.

The orbitals obtained are shown in Figs. 3 and 4 for the dimer and monomer-based cluster anions, respectively. Examining the monomer-based structures, it is apparent that solvation with one molecule of water, carbon dioxide, or indeed both, makes little difference to the shape of the HOMO. The symmetry of the dimer anion [Fig. 3(a.1)] is altered due to structural distortion induced by the water molecule and in the structure shown in Fig. 3(b.2) there is a slight localization of the negative charge toward the water-solvated end of the $(CO_2)_2^-$ unit. However, these are small effects and the HOMO remains essentially the same. Hence, the similarities of the PADs from monohydrated and nonhydrated cluster anions with similar cores are not surprising.

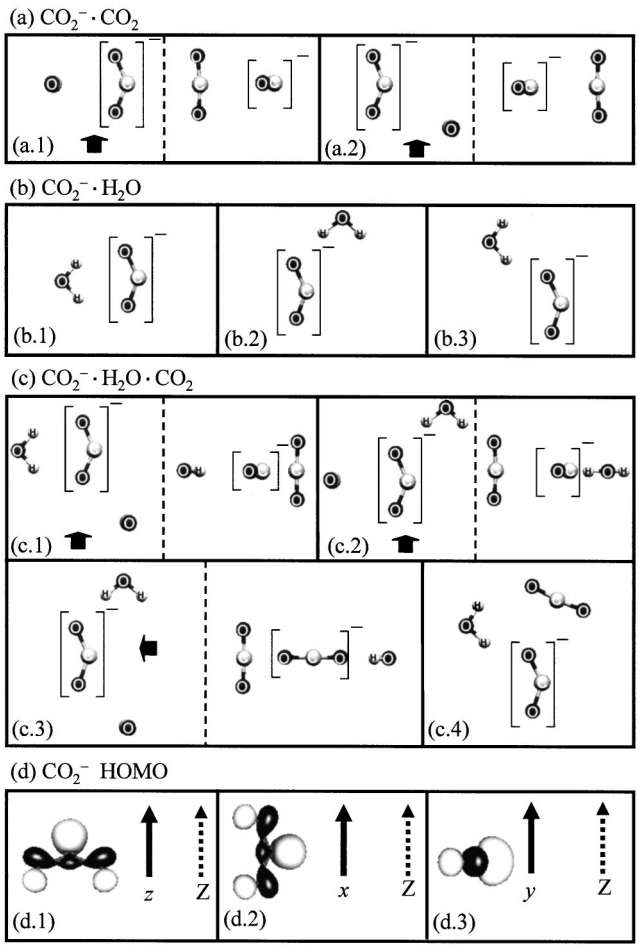

FIG. 4. Stable monomer-based cluster anion structures calculated at the MP2 level of theory with the 6-31+G* basis set (Ref. 23). Two projections are shown for the nonplanar structures in (a.1-2) and (c.1-3), with the viewpoint for the second projection indicated in the first by a wide arrow. The anionic core within each structure is indicated by square brackets. (a) The $CO_2^- \cdot CO_2$ cluster anion: (a.1) C_{2v} symmetry structure; (a.2) C_s symmetry structure. (b) The $CO_2^- \cdot H_2O$ cluster anion: (b.1) C_{2v} symmetry structure; (b.2-3) C_s symmetry structures, of which (b.2) is predicted to lie lower in energy. (c) The $CO_2^- \cdot CO_2 \cdot H_2O$ cluster anion: the structures in (c.1)–(c.3) have the solvating CO_2 molecule perpendicular to the plane of the $CO_2 \cdot H_2O$ unit, while in (c.4) the whole cluster is planar. (c.1) is the lowest energy structure, followed by (c.2), (c.3), and finally (c.4). (d) The plot of the CO_2^- HOMO shown in the three principal orientations used in the *s*&*p* model. Each orientation corresponds to one of the molecular-frame axes (x,y,z) aligned along the laboratory z axis, defined as the laser polarization direction. The shape of the monomer HOMO is largely unchanged in all of the cluster structures shown.

V. SUMMARY

The results of the photoelectron imaging experiments are in good agreement with previous work in regard to the energetics of photodetachment from $(CO_2)_n^-$ and $(CO_2)_n^- \cdot H_2O$ clusters. Evidence is seen for two different types of cluster core (monomer and covalent-dimer anions of CO_2). In addition, the imaging approach has allowed a systematic study of the photoelectron angular distributions, which reflect the orbital nature of the different core structures. Analysis of the PADs shows that solvation of the monomer CO_2^- and dimer $(CO_2)_2^-$ units by neutral CO_2 molecules has only a moderate effect on structure of the excess electron within the clusters. Likewise, the presence of a single water molecule makes little difference in this respect. The most intriguing result is that the PADs obtained from clusters with different ionic core types show striking similarities. These findings are supported by theoretical calculations and modeling the photodetachment from the covalent dimer anion using an LCMO description of the parent anion HOMO coupled with a dual-source wave interference model.

ACKNOWLEDGMENTS

We would like to acknowledge helpful discussions with Professor Mark A. Johnson. This work is supported by the NSF Grant No. CHE-0134631, the Beckman Young Investigator Award (The Arnold and Mabel Beckman Foundation), and the Packard Fellowship for Science and Engineering (The David and Lucile Packard Foundation).

[1] K. M. Ervin and W. C. Lineberger, in *Advances in Gas Phase Ion Chemistry*, edited by N. G. Adams and L. M. Babcock (JAI Press, Greenwich, 1992), Vol. 1, p. 121.
[2] A. W. Castleman and S. Wei, Annu. Rev. Phys. Chem. **45**, 685 (1994).
[3] A. W. Castleman and K. H. Bowen, J. Phys. Chem. **100**, 12911 (1996).
[4] A. Sanov and W. C. Lineberger, Phys. Chem. Comm. **5** , 165 (2002).
[5] D. W. Chandler and P. L. Houston, J. Chem. Phys. **87**, 1445 (1987).
[6] A. J. R. Heck and D. W. Chandler, Annu. Rev. Phys. Chem. **46**, 335 (1995).
[7] E. Surber and A. Sanov, J. Chem. Phys. **116**, 5921 (2002).
[8] R. Mabbs, E. Surber, and A. Sanov, Analyst **128**, 765 (2003).
[9] E. Surber, R. Mabbs, and A. Sanov, J. Phys. Chem. A **107**, 8215 (2003).
[10] E. Surber and A. Sanov, J. Chem. Phys. **118**, 9192 (2003).
[11] E. Surber and A. Sanov, Phys. Rev. Lett. **90**, 093001 (2003).
[12] T. Tsukuda, T. Hirose, and T. Nagata, Chem. Phys. Lett. **279**, 179 (1997).
[13] A. Sanov, S. Nandi, K. D. Jordan, and W. C. Lineberger, J. Chem. Phys. **109**, 1264 (1998).
[14] R. Mabbs, E. Surber, and A. Sanov, Chem. Phys. Lett. **381**, 479 (2003).
[15] M. J. DeLuca, B. Niu, and M. A. Johnson, J. Chem. Phys. **88**, 5857 (1988).
[16] T. Nagata, H. Yoshida, and T. Kondow, Chem. Phys. Lett. **199**, 205 (1992).
[17] T. Tsukuda, M. A. Johnson, and T. Nagata, Chem. Phys. Lett. **268**, 429 (1997).
[18] T. Tsukuda, M. Saeki, R. Kimura, and T. Nagata, J. Chem. Phys. **110**, 7846 (1999).
[19] T. Nagata, H. Yoshida, and T. Kondow, Z. Phys. D: At., Mol. Clusters **26**, 367 (1993).
[20] M. Saeki, T. Tsukuda, and T. Nagata, Chem. Phys. Lett. **340**, 376 (2001).
[21] M. Saeki, T. Tsukuda, and T. Nagata, Chem. Phys. Lett. **348**, 461 (2001).
[22] S. H. Fleischman and K. D. Jordan, J. Phys. Chem. **91**, 1300 (1987).
[23] M. Saeki, T. Tsukuda, S. Iwata, and T. Nagata, J. Chem. Phys. **111**, 6333 (1999).
[24] E. Surber, R. Mabbs, T. Habteyes, and A. Sanov (unpublished).
[25] M. A. Johnson and W. C. Lineberger, in *Techniques for the Study of Ion Molecule Reactions*, edited by J. M. Farrar and W. H. Saunders (Wiley, New York, 1988), p. 591.
[26] M. E. Nadal, P. D. Kleiber, and W. C. Lineberger, J. Chem. Phys. **105**, 504 (1996).
[27] A. T. J. B. Eppink and D. H. Parker, Rev. Sci. Instrum. **68**, 3477 (1997).
[28] W. C. Wiley and I. H. McLaren, Rev. Sci. Instrum. **26**, 1150 (1955).
[29] V. Dribinski, A. Ossadtchi, V. A. Mandelshtam, and H. Reisler, Rev. Sci. Instrum. **73**, 2634 (2002).
[30] J. Cooper and R. N. Zare, in *Atomic Collision Processes*, edited by S. Geltman, K. T. Mahanthappa, and W. E. Brittin (Gordon and Breach, Science Publishers, New York, London, Paris, 1968), Vol. XI-C, p. 317.
[31] J. Cooper and R. N. Zare, J. Chem. Phys. **48**, 942 (1968).
[32] J. Cooper and R. N. Zare, J. Chem. Phys. **49**, 4252 (1968).
[33] M. J. S. Dewar, Proc. Cambridge Philos. Soc. **45**, 638 (1949).
[34] L. L. Combs, Int. J. Quantum Chem. **11**, 1001 (1977).
[35] M. J. Frisch *et al.*, GAUSSIAN 98 Gaussian, Inc., Pittsburgh, PA, 1998.